An Investigation into the Characteristics of Nonlinear Frequency Response Functions, Part 2: New Analysis Methods Based on Symbolic Expansions and Graphical Techniques

R.Yue, S.A.Billings and Zi-Qiang Lang

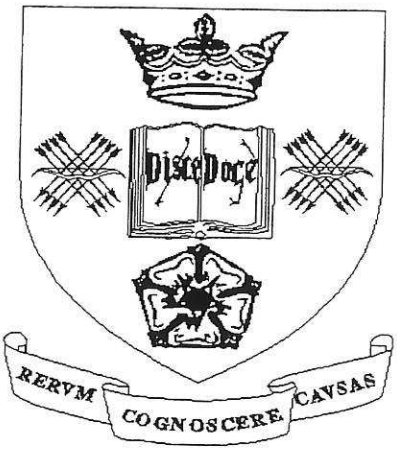

Department of Automatic Control and Systems Engineering
The University of Sheffield
Sheffield S1 3JD
U.K.

Research Report No.855
March 2004

An Investigation into the Characteristics of Nonlinear Frequency Response Functions, Part 2: New Analysis Methods Based on Symbolic Expansions and Graphical Techniques

R.Yue, S.A.Billings and Zi-Qiang Lang

Department of Automatic Control and Systems Engineering,
The University of Sheffield, Sheffield S1 3JD,U.K.

Abstract

In Part 1 of this paper the concepts of input and output frequency subdomains were introduced to give insight into the relation between one dimensional and multi-dimensional frequency spaces. The visualisation of both magnitude and phase responses of third order generalised frequency response functions was also presented. In this, the second part, symbolic expansion techniques are introduced and together with the results achieved in Part 1, yield new methods for analysing the properties of generalised frequency response functions. Case studies are included to illustrate the application of the new methods.

Keywords: Nonlinear Systems, Generalized Frequency Response Functions, Frequency Domain Analysis

1. Introduction

The great success of linear frequency domain analysis for describing the dynamic behaviour and assessing system stability in the linear systems case can be attributed to the simple analytical expressions and the transparent relationship between time and frequency domain behaviours. Intuitively therefore if the closed-from expressions for the generalised response functions of a class of nonlinear systems could be obtained, a similar analysis might be carried out on the properties of the GFRFs and an extension of the whole methodology of linear systems in the frequency domain to the nonlinear case may be possible. The method proposed by Billings and Tsang (1989a) for evaluating the GFRFs provides such a possibility. The approach involves estimating a discrete-time polynomial NARMAX model of a nonlinear system and obtaining the GFRFs directly by probing the model. The closed form of analytical expressions for the GFRFs can be obtained with this approach. Later, Peyton Jones and Billings (1989) completed this approach by developing a recursive algorithm for computer implementation. In this, Part 2 of the paper, the results from those previous studies will be used and combined with symbolic computations and graphical techniques in higher dimensions to give a unified study of the properties of the GFRFs for a broad class of nonlinear systems. Case study examples are included to illustrate the effectiveness of the new methods. For the sake of completeness, the parametric model based method for estimating the GFRFs are briefly reviewed first. The map from wavelet NARMAX models to GFRFs has also been derived by Boaghe and Billings (2000) but these results will not be discussed here.

2. Investigating the GFRFs Using Symbolic Expansions and Graphical Techniques in Higher Dimensions

2.1 The NARX Model and Generalised Frequency Response Functions

A wide class of nonlinear systems can be described by the NARMAX (Nonlinear AutoRegressive Moving Average with eXogenous inputs) model (Leontaritis and Billings 1985)

$$y(t) = F[y(t-1),\cdots,y(t-k_y),u(t-1),\cdots,u(t-k_u),\zeta(t-1),\cdots,\zeta(t-k_\zeta)] \tag{2.1}$$

where $F[\cdot]$ denotes some discrete nonlinear function of the lagged input signals $u(t-k_u)$, outputs $y(t-k_y)$, and noise $\zeta(t-k_\zeta)$; t is used to enumerate the sampling intervals and k the lags. Algorithms for detecting the model structure, estimating the parameters and validating these models have been well developed (Korenberg et al 1988, Billings et al 1988) and have been used to identify many physical systems from real plant data.

Once this identification process is complete, the moving average noise terms (which were included to ensure unbiased estimation) may be discarded, yielding a deterministic 'NARX' model containing input and output terms only. The polynomial structural form of the NARX model can be described by

$$y(k) = \sum_{m=1}^{M} y_m(k) \tag{2.2}$$

where $y_m(k)$, the NARX mth-order output of the system, is given by

$$y(k) = \sum_{p=0}^{m} \sum_{k_1,k_{p+q}=1}^{K} c_{p,q}(k_1,\cdots,k_{p+q}) \prod_{i=1}^{p} y(k-k_i) \prod_{i=p+1}^{p+q} u(k-k_i) \tag{2.3}$$

with $p+q=m,\ k_i=1,\cdots,p+q,\ and\ \sum_{k_1,k_{p+q}=1}^{K} \equiv \sum_{k_1}^{K}\cdots\sum_{k_{p+q}}^{K}$. Notice that each term in (2.3) contains a pth-order factor in $y(k-k_i)$ and a qth-order factor in $u(k-k_i)$ and is multiplied by the coefficient $c_{p,q}(k_1,\cdots,k_{p+q})$.

The successive generalized frequency response functions can be obtained (Billings and Tsang 1989a) and the recursive computation formula of these is given by (Peyton and Billings 1989):

$$\begin{aligned}
&\left(1-\sum_{k_1=1}^{K} c_{1,0}(k_1)\ e^{-j(\varpi_1+\cdots+\varpi_n)k_1}\right) H_n^{asym}(j\varpi_1,\cdots,j\varpi_n) \\
&= \sum_{k_1,k_n=1}^{K} c_{0,n}(k_1,\cdots,k_n)\ e^{-j(\varpi_1 k_1+\cdots+\varpi_n k_n)} \\
&+ \sum_{q=1}^{n-1}\sum_{p=1}^{n-q}\sum_{k_1,k_n=1}^{K} c_{p,q}(k_1,\cdots,k_{p+q})\ e^{-j(\varpi_{n-q+1}k_{n-q+1}+\cdots+\varpi_{p+q}k_{p+q})}\ H_{n-q,p}(j\varpi_1,\cdots,j\varpi_{n-q}) \\
&+ \sum_{p=2}^{n}\sum_{k_1,k_p=1}^{K} c_{p,0}(k_1,\cdots,k_p)\ H_{n,p}(j\varpi_1,\cdots,j\varpi_n)
\end{aligned} \tag{2.4}$$

where $H_{n,p}(j\varpi_1,\cdots,j\varpi_n)$ is given by

$$H_{n.p}^{asym}(j\varpi_1,\cdots,j\varpi_n)=\sum_{i=1}^{n-p+1}H_i(j\varpi_1,\cdots,j\varpi_i)H_{n-i,p-1}(j\varpi_{i+1},\cdots,j\varpi_n)\ \ e^{-j(\varpi_1+\cdots+\varpi_i)k_p} \quad (2.5)$$

The recursion in the above equation finishes with p=1 where $H_{n,1}(j\varpi_1,\cdots,j\varpi_n)$ has the property

$$H_{n.1}(j\varpi_1,\cdots,j\varpi_n)=H_n(j\varpi_1,\cdots,j\varpi_n)\ \ e^{-j(\varpi_1+\cdots+\varpi_n)k_1} \quad (2.6)$$

Note that (2.4) gives the asymmetric generalised frequency response functions, although it is a simple matter to obtain unique symmetric values by adding all the asymmetric GFRFs over all permutations of the arguments and dividing by the number (Schetzen 1980) to give.

$$H_n^{sym}(j\varpi_1,\cdots,j\varpi_n)=\frac{1}{n!}\sum_{\substack{all\ permutations\\ of\ \varpi_1\cdots\varpi_n}}H_n(j\varpi_1,\cdots,j\varpi_n) \quad (2.7)$$

2.2 Symbolic Expansion Of the GFRFs and the Interpretation of the Basic Elements

Equation (2.4) provides a means of obtaining the higher order GFRFs in terms of the lower order functions. This parametric method has particular significance in the sense that closed form expressions involving the parameters of the system time domain model are obtained and this makes it possible to investigate the link between the system time domain dynamic behaviour and the characteristics of the GFRFs. However, as noted in the introduction, the structure of the GFRFs remain concealed in this recursive form, which limits further exploitation of significant results in the frequency domain analysis of nonlinear systems. While it is straightforward to tackle this problem by directly expanding the recursive expression of (2.4), exercising such manipulations by pen and paper can be tedious and hard work especially when dealing with higher order functions. In this study, symbolic computations will be used to automatically derive the fundamental structure of the GFRFs from (2.4). In symbolic computations the basic data type for representing the mathematical quantities is a character string or formula rather than a sequence of numerical values and the mathematical information and structure of the model are therefore retained. Most importantly, the final results obtained in this way, for the first time, clearly show how the structure and properties of the GFRFs depend on the parameters of the system model.

To illustrate the development, consider a nonlinear system described by the NARX model with a quadratic nonlinearity in the output,

$$y(k)=\underbrace{0.7y(k-1)}_{\substack{linear\ output\ term1\\ p=1,q=0\\ lag1=1}}+\underbrace{0.3u(k-1)}_{\substack{linear\ input\ term1\\ p=0,q=1\\ lag1=1}}-\underbrace{0.08y(k-1)y(k-3)}_{\substack{pure\ output\ nonlinearity\ of\ Degree2\ term\ 1\\ p=2,q=0\\ lag1=1,lag\ 2=3}} \quad (2.8)$$

which is a specific instance of the general NARX model (2.3) with

$$c_{1,0}(1)=0.7,\ c_{0,1}(1)=0.3,\ c_{2,0}(1,3)=-0.08 \quad (2.9)$$

For convenience in the symbolic manipulations, a slightly modified notation will be introduced to denote the coefficients and lags of each term in the NARX model (2.3), which, using the new notation, becomes

$$y(k)=\sum_{\substack{p=0\\ p+q=m}}^{m}\sum_{\substack{h=1\\ k_{pq\succ h\_1}\in1,\cdots,K\\ \vdots\\ k_{pq\succ h\_p+q}\in1,\cdots,K}}^{L}c_{pq\succ h}\prod_{i=1}^{p}y(t-k_{pq\succ h\_i})\prod_{i=p+1}^{p+q}u(t-k_{pq\succ h\_i}) \quad (2.10)$$

where the subscript $pq\succ h$ means the hth term in the class of terms with p output factors and q input factors. Correspondingly the coefficient and the ith lag of this term are denoted by

$c_{pq>h}$ and $k_{pq>h\_i}$ respectively. To make this clear, the NARX model (2.8) is re-written in this manner as,

$$y(k) = c_{10>1}y(k-k_{10>1\_1}) + c_{01>1}u(k-k_{01>1\_1}) + c_{20>1}y(k-k_{20>1\_1})y(k-k_{20>1\_2}) \tag{2.11}$$

where

$$\begin{aligned} &c_{10>1} = c_{1,0}(1) = 0.7,\ c_{01>1} = c_{0,1}(1) = 0.3,\ c_{20>1} = c_{2,0}(1,3) = -0.08 \\ &k_{10>1\_1} = 1,\ k_{01>1\_1} = 1,\ k_{20>1\_1} = 1,\ k_{20>1\_2} = 3 \end{aligned} \tag{2.12}$$

From (2.4), the first, second and third order frequency response functions of the system (2.8) are given by

$$H_1(j\varpi_1) = \frac{c_{01>1}\exp(-j\ \ k_{01>1\_1}\varpi_1)}{1-c_{10>1}\exp(-j\ \ k_{10>1\_1}\varpi_1)} \tag{2.13}$$

$$H_2^{asym}(j\varpi_1, j\varpi_2) = \frac{c_{20>1}H_1(j\varpi_1)H_1(j\varpi_2)\exp[-j\ \ (k_{20>1\_2}\varpi_1 + k_{20>1\_1}\varpi_2)]}{1-c_{10>1}\exp[-j\ \ k_{10>1\_1}(\varpi_1+\varpi_2)]} \tag{2.14}$$

$$\begin{aligned} H_3^{asym}(j\varpi_1, j\varpi_2) = c_{20>1}\{&H_1(j\varpi_1)H_2(j\varpi_2, j\varpi_3)\exp[-j\ \ (k_{20>1\_2}\varpi_1 + k_{20>1\_1}(\varpi_2+\varpi_3)] \\ &+H_1(j\varpi_3)H_2(j\varpi_1, j\varpi_2)\exp[-j\ \ (k_{20>1\_2}(\varpi_1+\varpi_2) + k_{20>1\_1}\varpi_3)]\} \\ &/\{1-c_{10>1}\exp[-j\ \ k_{10>1\_1}(\varpi_1+\varpi_2+\varpi_3)]\} \end{aligned} \tag{2.15}$$

where ω_1, ω_2 and ω_3 are frequency variables. FigsFig. 1, Fig. 2 and Fig. 3 show the H_1, H_2 and H_3 above respectively. Both the expression and the plot for the first order frequency response H_1 are straightforward and can be well understood from a knowledge of linear systems theory. Fig. 1 indicates that the linear frequency response of the system (2.8) behaves like a low pass system with gain at zero frequency equal to unity. Unfortunately the higher order GFRFs H_2 and H_3 are not transparent due to the recursive form in equation (2.14) and (2.15). This makes it difficult to investigate the properties of H_2 and H_3 and or to give a simplified explanation of the sophisticated plots shown in FigsFig. 2 and Fig. 3. Symbolic manipulation can be employed to substitute the lower order GFRFs into the expressions of the higher order GFRFs and to perform the complicated procedure of simplification to obtain the expanding forms of expressions (2.14) and (2.15). These are given by

$$\begin{aligned} &H_2^{asym}(j\varpi_1, j\varpi_2) = \\ &\frac{c_{20>1}c_{01>1}^2\exp\{-j\ \ [(k_{10>1\_1}+k_{20>1\_2})\varpi_1 + (k_{10>1\_1}+k_{20>1\_1})\varpi_2]\}}{[1-c_{10>1}\exp(-j\ \ k_{10>1\_1}\varpi_1)]\ [1-c_{10>1}\exp(-j\ \ k_{10>1\_1}\varpi_2)]\ \{1-c_{10>1}\exp[-j\ \ k_{10>1\_1}(\varpi_1+\varpi_2)]\}} \end{aligned} \tag{2.16}$$

$$H_3^{asym}(j\varpi_1, j\varpi_2, j\varpi_3) = c_{20\text{>}1}^2 c_{01\text{>}1}^3 \times$$

$$\left\{\begin{array}{l}
\exp\{-j\ \ [(k_{01\text{>}1_1}+k_{20\text{>}1_2})\varpi_1+(k_{10\text{>}1_1}+k_{20\text{>}1_1}+k_{20\text{>}1_2})\varpi_2 \\
\ \ +(k_{10\text{>}1_1}+2k_{20\text{>}1_1})\varpi_3]\} \\
+\exp\{-j\ \ [(k_{01\text{>}1_1}+2k_{20\text{>}1_2})\varpi_1+(k_{10\text{>}1_1}+k_{20\text{>}1_1}+k_{20\text{>}1_2})\varpi_2 \\
\ \ +(k_{01\text{>}1_1}+k_{20\text{>}1_1})\varpi_3]\} \\
-c_{10\text{>}1}\times\exp\{-j\ \ [(k_{01\text{>}1_1}+k_{10\text{>}1_1}+k_{20\text{>}1_2})\varpi_1+ \\
\ \ (k_{01\text{>}1_1}+k_{10\text{>}1_1}+k_{20\text{>}1_1}+k_{20\text{>}1_2})\varpi_2+(k_{01\text{>}1_1}+2k_{20\text{>}1_1})\varpi_3]\} \\
-c_{10\text{>}1}\times\exp\{-j\ \ [(k_{01\text{>}1_1}+2k_{20\text{>}1_2})\varpi_1+ \\
\ \ (k_{01\text{>}1_1}+k_{10\text{>}1_1}+k_{20\text{>}1_1}+k_{20\text{>}1_2})\varpi_2+(k_{01\text{>}1_1}+k_{10\text{>}1_1}+k_{20\text{>}1_1})\varpi_3]\} \\
\hline
[1-c_{10\text{>}1}\exp(-j\ \ k_{10\text{>}1_1}\varpi_1)]\times[1-c_{10\text{>}1}\exp(-j\ \ k_{10\text{>}1_1}\varpi_2)]\times[1-c_{10\text{>}1}\exp(-j\ \ k_{10\text{>}1_1}\varpi_3)] \\
\times\{1-c_{10\text{>}1}\exp[-j\ \ k_{10\text{>}1_1}(\varpi_1+\varpi_2)]\}\times\{1-c_{10\text{>}1}\exp[-j\ \ k_{10\text{>}1_1}(\varpi_2+\varpi_3)]\} \\
\times\{1-c_{10\text{>}1}\exp[-j\ \ k_{10\text{>}1_1}(\varpi_1+\varpi_2+\varpi_3)]\}
\end{array}\right. \tag{2.17}$$

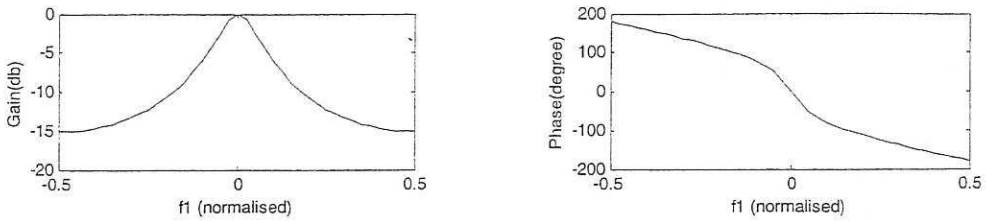

(a) magnitude (b) Phase

Fig. 1 The first order generalised frequency response function H_1 of the nonlinear system (2.8)

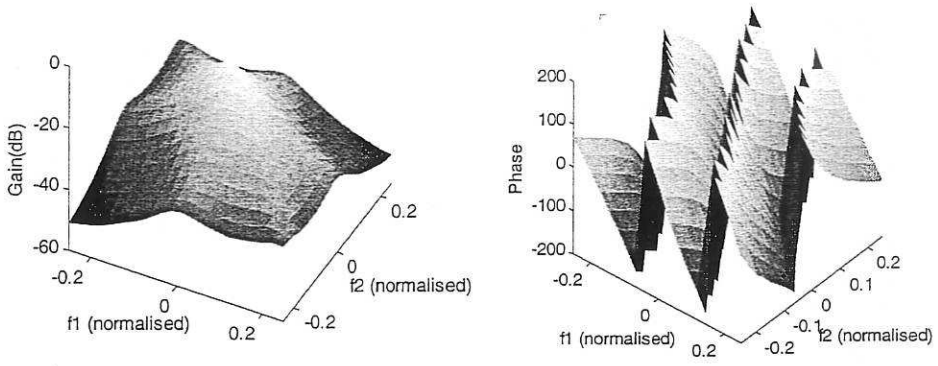

(a) magnitude (b) Phase

Fig. 2 The second order generalised frequency response function H_2 of the nonlinear system (2.8)

The obvious advantage of expressing the GFRFs in expanded form is that this explicitly reveals the relationship between the time-domain model parameters and the GFRFs of a nonlinear system. Hence the contributing effect of individual time domain terms on the properties of GFRFs becomes explicit. As will be seen later, a small change in the coefficient or the lag of some terms in the time-domain model can result in a new set of GFRFs with totally different properties, which in turn produce distinct nonlinear effects for a fixed input. Observe that the expanding forms of H_2 and H_3 along with the expression of H_1 display a similar structure and can be written as follows in a unified form

$$H_n^{asym}(j\varpi_1,\cdots,j\varpi_n)=\frac{\sum_{l=1}^{R} c_l \exp[-j \sum_{i=1}^{n} k_l^i \varpi_i]}{\prod_{i=1}^{n}[1-c_{10>1}\exp(-j\ k_{10>1\_1}\varpi_i)]\cdots \prod_{i=1}^{g}\{1-c_{10>1}\exp[-j\ k_{10>1\_1}(\varpi_{l_i}^{r_1}+\cdots+\varpi_{l_i}^{r_m})]\}\cdots \{1-c_{10>1}\exp[-j\ k_{10>1\_1}(\varpi_1+\cdots+\varpi_n)]\}} \tag{2.18}$$

where the coefficients of the exponential terms in the numerator, $c_1,\cdots,c_R$ are decided solely by the coefficients of the terms in the time-domain model $c_{10\succ1}$, $c_{01\succ1}$ and $c_{20\succ1}$ while the lags in the time-domain model $k_{10\succ1\_1}$, $k_{01\succ1\_1}$, $k_{20\succ1\_1}$ and $k_{20\succ1\_2}$ alone contribute to the coefficients, $(k_1^1,\cdots,k_1^n),\cdots,(k_n^1,\cdots,k_n^n)$ which are associated with frequency variables in the numerator. The constant g in the denominator of equation (2.18) is the number of the terms in the form of an m-variable function $1-c_{10\succ1}\exp[-jk_{10\succ1\_1}(\varpi_{l_i}^{r_1}+\cdots+\varpi_{l_i}^{r_m})]$, where $(\varpi_{l_i}^{r_1},\cdots,\varpi_{l_i}^{r_m})$ is a subset of $(\varpi_1,\cdots,\varpi_n)$ with m elements. In general, g will be less than the total number of the combination of n frequencies taken m at a time. The inequality becomes an equality when the symmetric form of the GFRF is considered. Clearly the denominator in (2.18) is determined only by the linear output terms.

For a deep insight into the structure of an *nth*-order GFRF as well as the dependence of the GFRF on the model coefficients, the right-hand side of equation (2.18) can be further decomposed into some basic elements,

- *The summation of exponential phasors:* $\sum_{l=1}^{R}c_l\exp[-j\sum_{i=1}^{n}k_l^i\varpi_i]$, *which determines the minima of the nth-order GFRF*
- *The factors in the denominator, which jointly determine the maxima of the nth-order GFRF:*

(i). $\dfrac{1}{1-c_{10\succ1}\exp(-jk_{10\succ1\_1}\varpi_i)}, i=1,\cdots,n$, *which are n-dimensional functions dependent only on one of n frequency variables.*

(ii). $\dfrac{1}{1-c_{10\succ1}\exp[-jk_{10\succ1\_1}(\varpi_{r_1}+\cdots+\varpi_{r_m})]}$, *which are n-dimensional functions dependent on m distinct frequency variables taken from* $(\varpi_1,\cdots,\varpi_n)$

(iii). $\dfrac{1}{1-c_{10\succ1}\exp[-jk_{10\succ1\_1}(\varpi_1+\cdots+\varpi_n)]}$, *which is an n-variable function*

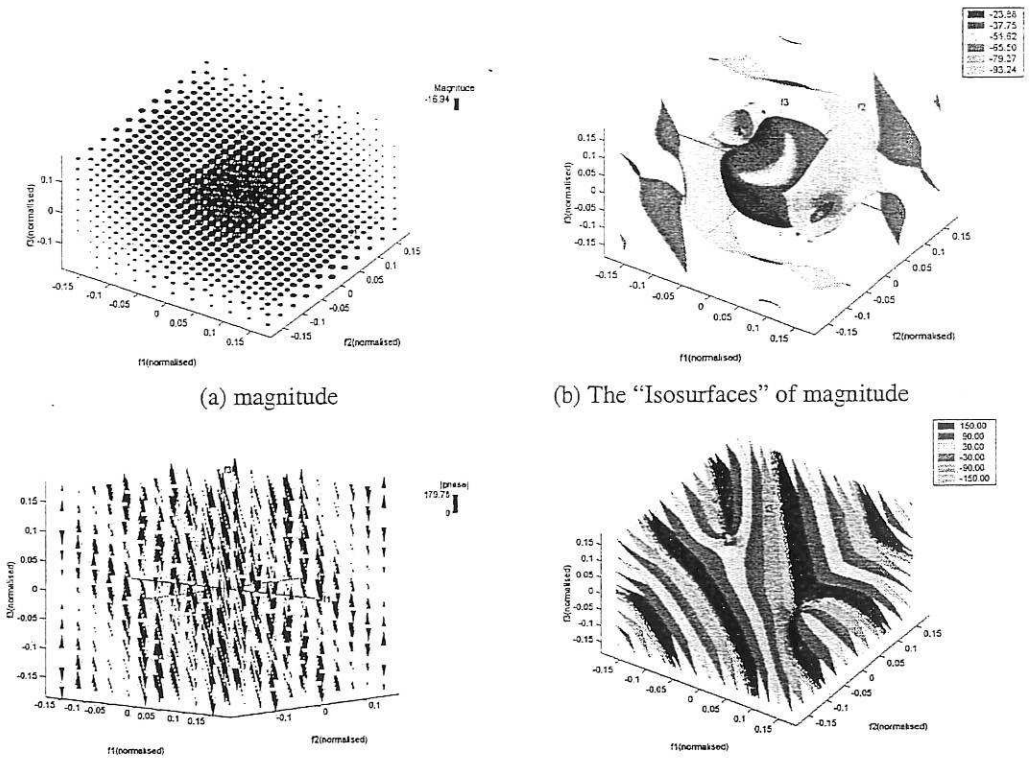

(a) magnitude (b) The "Isosurfaces" of magnitude

(c) phase (d) The "Isosurfaces" of phase

Fig. 3 The third order generalised frequency response function H_3 of the nonlinear system (2.8)

These elements provide a means of interpreting the complicated plots of the higher order GFRFs. For the second order GFRF H_2 in this case, substituting the numerical values of the coefficients into (2.16), the corresponding basic elements in (2.16) can be obtained straightway as follows:

The exponential phasor: $$0.0072\exp[-j\ (4\varpi_1+2\varpi_2)] \quad (2.19)$$

The factors in the denominator: $$\left\{\frac{1}{1-0.7\exp(-j\varpi_1)}, \frac{1}{1-0.7\exp(-j\varpi_2)}, \frac{1}{1-0.7\exp[-j(\varpi_1+\varpi_2)]}\right. \quad (2.20)$$

Fig. 4 shows the gain and phase plots of the basic elements above. If $1/[1-0.7\exp(-j\varpi_1)]$ is defined as a one-dimensional function, the gain plot is exactly the same as the gain plot of H_1 shown in Fig. 1(a). The gain plot of the factor $1/[1-0.7\exp(-j\varpi_1)]$ in (2.20), which is defined as a two-dimensional function dependent only on the variable ϖ_1, can be viewed as the extension of Fig. 1(a) to a two-dimensional space. Any plane defined by ω_2=*constant* in Fig. 4(a) is the same as Fig. 1(a). Similarly, for the gain plots of $1/[1-0.7\exp(-j\varpi_2)]$ and $1/\{1-0.7\exp[-j(\varpi_1+\varpi_2)]\}$, any slice cut by

$\omega_1 = constant$ and $\omega_1 = \omega_2 + constant$ displays the same curve as in Fig. 1(a). Since a logarithm scale is employed in calculating the magnitude frequency response, the gain of H_2 is the sum of the gain of each individual element in (2.19) and (2.20). This fact is reflected in Fig. 2(a) and Fig. 4(a) (c) (e) (g), where it can be observed that the gain plot of H_2 is actually the superposition of the gain plots of all the basic elements. It follows that the three distinct ridges in Fig. 2(a) are the ridge along $\omega_1 = 0$ in Fig. 4(a), the ridge along $\omega_2 = 0$ in Fig. 4(c) and the ridge $\omega_1 + \omega_2 = 0$ in Fig. 4(e) respectively. The effect produced by the second order GFRF will first become significant at those peaks and ridges in Fig. 2(a), where the gain is at a maximum. The ridges corresponding to $\omega_1 = 0$ or $\omega_2 = 0$ indicate that there will be significant intermodulation effects on the output response if the input signal contains a significant d.c. bias while the ridge along $\omega_1 + \omega_2 = 0$, which corresponds to zero frequency in the output frequency domain described in §4, indicates that there will be a significant d.c.shift in the output response. The peak area close to the origin, which results from the intersection of these three ridges, indicates that there will be a strong intermodulation effect at low frequencies for low frequency excitations.

The features of the gain plot for H_2 can therefore be well understood based on this type of analysis. Note that the phasor in the numerator of (2.16) makes no contribution to the characteristics of the gain plot of H_2 and only affects the d.c. offset on the gain level. A superposition relation also exists between the phase plot of H_2 and the phase plots of the constituent elements due to the fact that the phase of the product of phasors is the sum of the phase of each phasor. Note that the main contribution to the features of the phase plot in H_2 comes from the phasor element in the numerator.

In the case where the symmetric form of H_2 is needed, an expression for H_2^{sym} can be given from (2.7) and (2.16) as follows,

$$H_2^{sym} = \frac{0.0036\{\exp[-j\ (4\varpi_1 + 2\varpi_2)] + \exp[-j\ (2\varpi_1 + 4\varpi_2)]\}}{[1-0.7\exp(-j\varpi_1)][1-0.7\exp(-j\varpi_2)]\{1-0.7\exp[-j(\varpi_1+\varpi_2)]\}} \tag{2.21}$$

which takes a very similar form to the asymmetric H_2. The only difference is that now the numerator is replaced by a sum of two phasors. This difference however results in a significant change to the gain and phase plots of H_2, which are shown in Fig. 5. Compared with Fig. 2(a), two deep gorges appear in the gain plot of the symmetric second order GFRF as seen in Fig. 5(a). The new features are generated by the numerator element of (2.21) where now the two phasors interact with each other. The gain plot of the numerator of (2.21) shown in Fig. 6(a) confirms the explanation above.

For the third-order GFRF, substituting the coefficients in (2.17) with numeric values and separating the basic elements gives the results below

- The numerator

$$\begin{aligned} &0.0001728\times\{\exp[-j\ (4\varpi_1 + 5\varpi_2 + 3\varpi_3)] + \exp[-j\ (7\varpi_1 + 5\varpi_2 + 2\varpi_3)] \\ &-0.7\times\{\exp[-j\ (5\varpi_1 + 6\varpi_2 + 3\varpi_3)] + \exp[-j(7\varpi_1 + 6\varpi_2 + 3\varpi_3)]\}\} \end{aligned} \tag{2.22}$$

- *The factors in the denominator*

(i) $1/[1-0.7\exp(-j\ \varpi_1)]$, $1/[1-0.7\exp(-j\ \varpi_2)]$, $1/[1-0.7\exp(-j\ \varpi_3)]$

(ii) $1/\{1-0.7\exp[-j\ (\varpi_1+\varpi_2)]\}$, $1/\{1-0.7\exp[-j\ (\varpi_2+\varpi_3)]\}$ (2.23)

(iii) $1/\{1-0.7\exp[-j\ (\varpi_1+\varpi_2+\varpi_3)]\}$

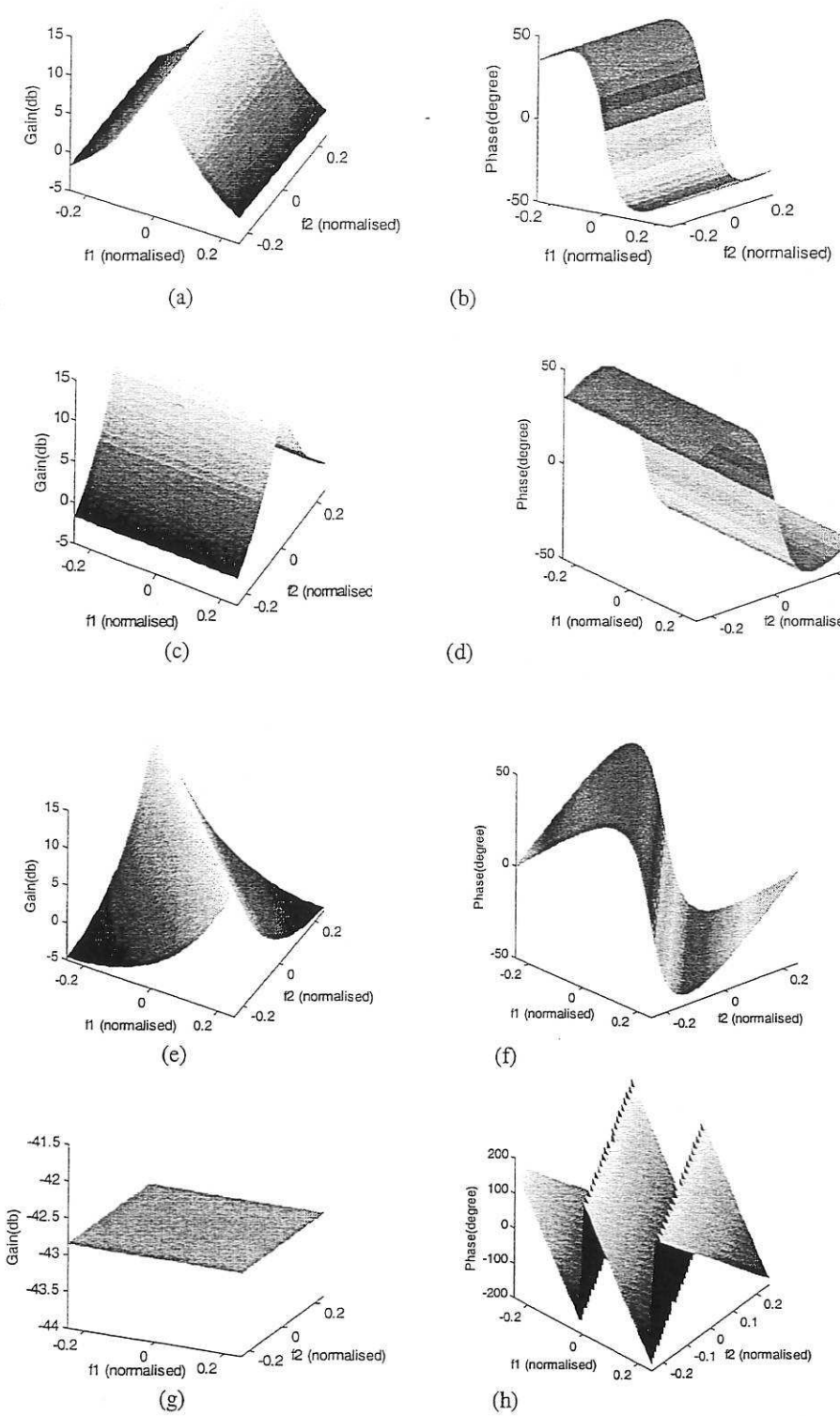

Fig. 4 (a)(b) the gain and phase plots of the element $1/[1-0.7\exp(-j\varpi_1)]$

(c)(d) the gain and phase plots of the element $1/[1-0.7\exp(-j\varpi_2)]$

(e)(f) the gain and phase plots of the element $1/[1-0.7\exp(-j(\varpi_1+\varpi_2))]$

(g)(h) the gain and phase plots of the element $0.0072\exp[-j\ (4\varpi_1+2\varpi_2)]$

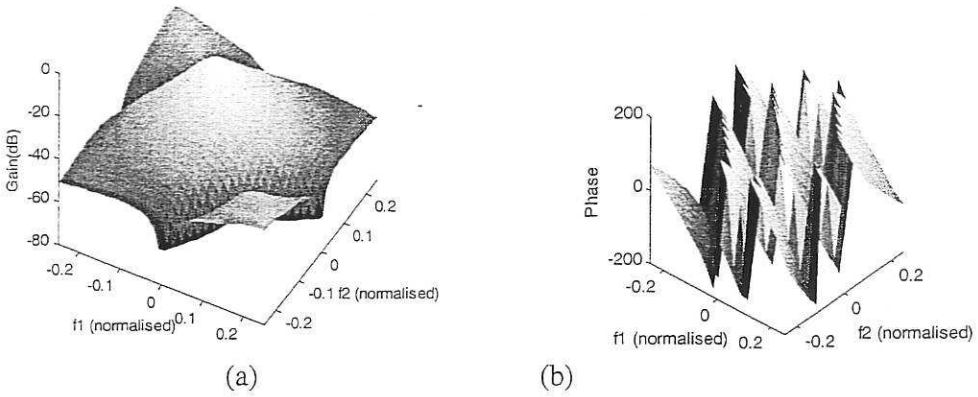

(a) (b)

Fig. 5 The gain and phase plots of H_2^{sym} given by (2.21). (a) gain; (b) phase

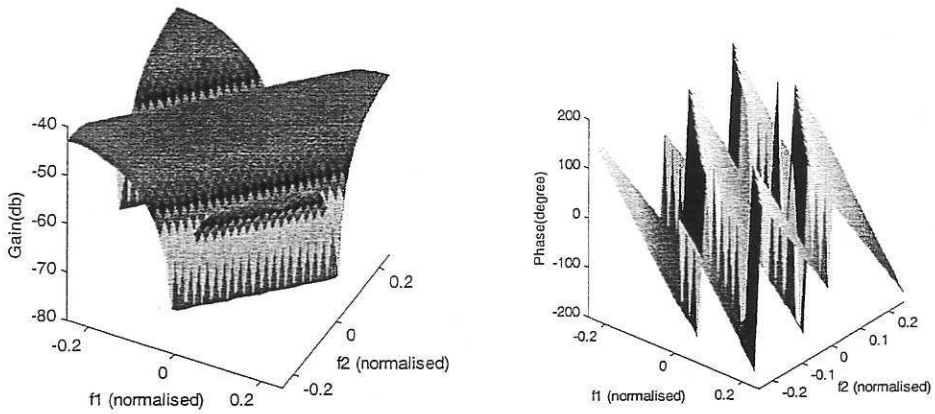

(c) (d)

Fig. 6 The gain and phase plots of the numerator element of (2.21). (a) gain; (b) phase

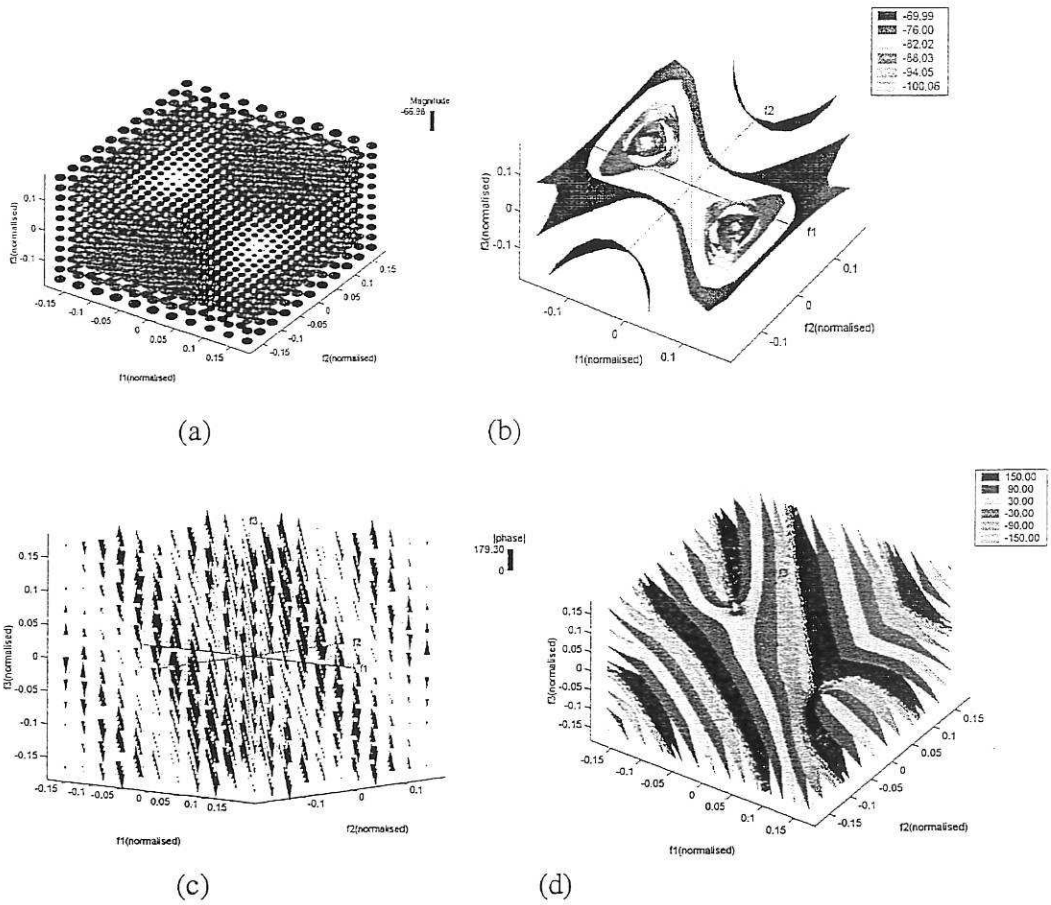

Fig. 7 The gain and phase plot of the numerator element of H_3^{asym} in (2.17)

$$0.0001728\times\{\exp[-j(4\varpi_1+5\varpi_2+3\varpi_3)]+\exp[-j(7\varpi_1+5\varpi_2+2\varpi_3)]$$
$$-0.7\times\{\exp[-j(5\varpi_1+6\varpi_2+3\varpi_3)]+\exp[-j(7\varpi_1+6\varpi_2+3\varpi_3)]\}\}$$

(a) The gain plot. (b) Isoplanes of the gain.
(c) The phase plot (d) Isoplanes of the phase

The numerator element (2.22) is shown in Fig. 7 and the factors in the denominator are displayed in Fig. 8. The plots of the basic elements reveal the individual features that are not evident in Fig. 3 where the whole third order GFRF is depicted. A prominent feature of the gain plot in Fig. 7 is the appearance of two distinct holes, which, like the two gorges in Fig. 6(a), are generated wherever the phasors in the numerator element cancel with each other. Note that Fig. 3(a) displays two holes at exactly the same position as in Fig. 7(a).

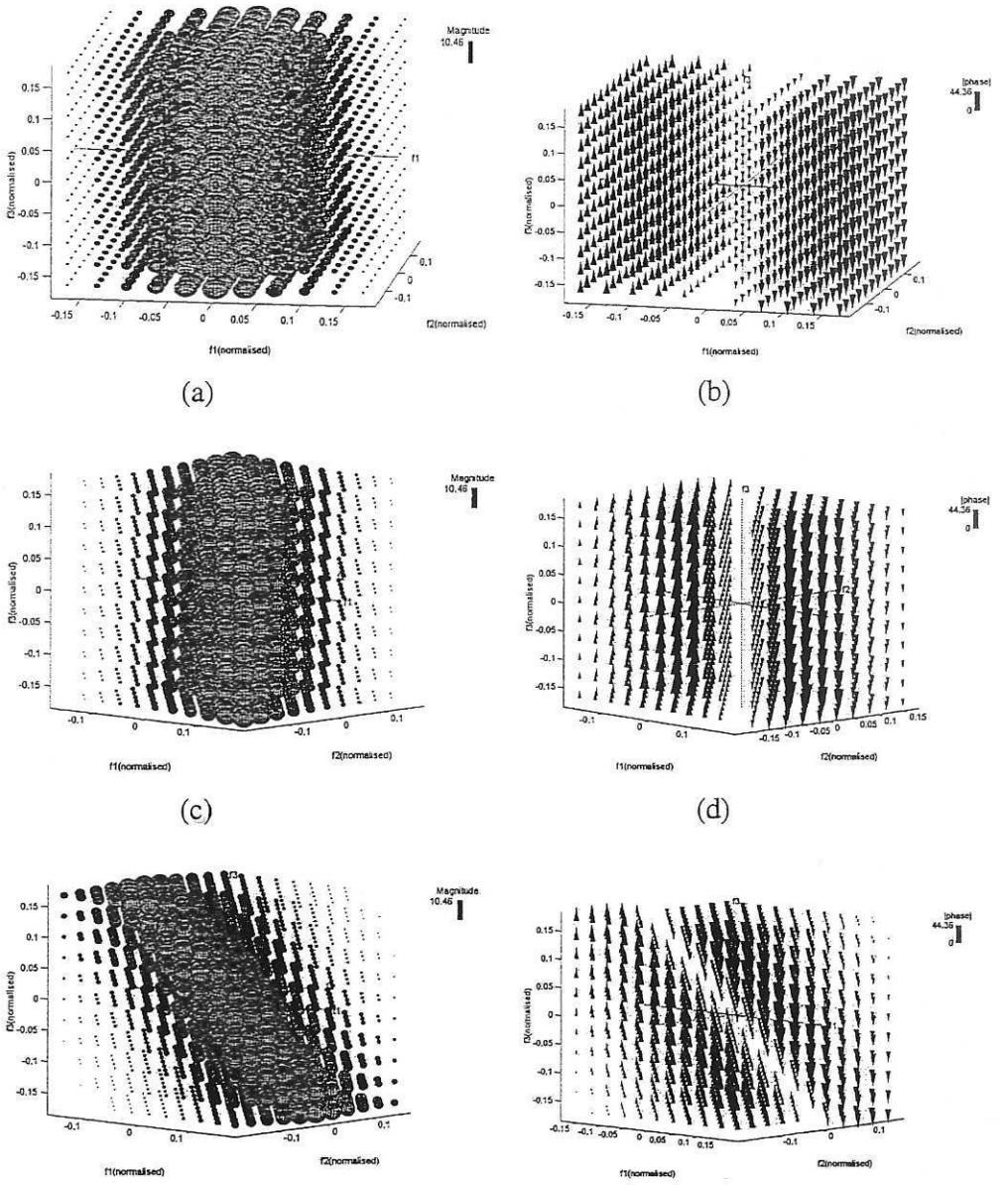

Fig. 8 The gain and phase plots of the elements in the denominator of $H_3^{asym}(j\varpi_1, j\varpi_2, j\varpi_3)$ for (2.17)

(a) (b) The gain and phase plots of the element $1/[1-0.7\exp(-j\varpi_1)]$

(c) (d) The gain and phase plots of the element $1/\{1-0.7\exp[-j(\varpi_1+\varpi_2)]\}$

(e) (f) The gain and phase plots of the element $1/\{1-0.7\exp[-j(\varpi_1+\varpi_2+\varpi_3)]\}$

The gain responses plotted in Fig. 8(a) (c) and (e) present the peak planes along $\omega_1 = 0$, $\omega_1 + \omega_2 = 0$ and $\omega_1 + \omega_2 + \omega_3 = 0$ where the corresponding gains reach maximum values. Similar peak planes also exist in the gains of other elements in the denominator which, for the sake of saving space, are not shown in Fig. 8. The peak planes indicate that the third order GFRF will produce strong nonlinear effects for an input with low frequency or d.c. components.

The analysis in this way can be readily extended to higher order GFRFs of three and above. In general, the expanded form of higher order GFRFs is obtained first and then the basic elements with simple forms are extracted. A clear image of higher order GFRF can finally be achieved through examining the features of each individual element.

The contributions of the terms in the system time domain model to the characteristics of the GFRFs have been made clear through the analysis above using a combination of symbolic expansions, decomposition and graphical techniques. While the coefficients and lags of the linear output terms together with nonlinear terms determine the prominent features of the magnitude of the GFRFs, which indicate where strong nonlinear intermodulations will take place, the nonlinear terms also contribute to the phase response. In order to assess such dependence of the GFRFs on the model structure and coefficients, it is important to see what changes in the model terms will have on the GFRFs. This can also easily be achieved using the methods above. For example, if $k_{10>1\_1}$, the lag of the linear output term in (2.11) is changed from 1 to 3, the GFRFs will present quite different features. In this case, the GFRFs of the first three orders become,

$$H_1 = \frac{0.3\exp(-j\ \varpi_1)}{1-0.7\exp(-j\ 3\varpi_1)} \tag{2.24}$$

$$H_2^{asym} = \frac{0.0072\exp[-j\ (4\varpi_1 + 2\varpi_2)]}{[1-0.7\exp(-j3\varpi_1)][1-0.7\exp(-j3\varpi_2)]\{1-0.7\exp[-j3(\varpi_1+\varpi_2)]\}} \tag{2.25}$$

$$H_3^{asym} = \frac{\begin{array}{l} 0.0001728\times\{\exp[-j\ (4\varpi_1+5\varpi_2+3\varpi_3)]+\exp[-j\ (7\varpi_1+5\varpi_2+2\varpi_3)] \\ -0.7\times\{\exp[-j\ (7\varpi_1+8\varpi_2+3\varpi_3)]+\exp[-j(7\varpi_1+8\varpi_2+5\varpi_3)]\}\} \end{array}}{\begin{array}{l} [1-0.7\exp(-j\ 3\varpi_1)]\ [1-0.7\exp(-j\ 3\varpi_2)][1-0.7\exp(-j\ 3\varpi_3)] \\ \{1-0.7\exp[-j\ 3(\varpi_1+\varpi_2)]\}\{1-0.7\exp[-j\ 3(\varpi_2+\varpi_3)]\} \\ \{1-0.7\exp[-j\ 3(\varpi_1+\varpi_2+\varpi_3)]\} \end{array}} \tag{2.26}$$

The linear output term dominates the structure of the basic elements in the denominator of the GFRFs and hence has a significant effect on the gain of the GFRFs. Fig. 9(a) shows the first order GFRF which now exhibits two resonant peaks at $\omega_1 = \pm 0.33$ in addition to the resonant peak at zero frequency in Fig. 1(a). The second order GFRF is shown in Fig. 9(c) where the ridges in Fig. 2(a) are replaced by new ridges as indicated by the marked curves B, C, D and E in Fig. 9(d), which also displays the corresponding contour plot.

Fig.20 (c) (d) and (e) shows the basic elements in the denominator of H_3. Compared to Fig. 8, the gains of the elements change considerably, especially the elements $1/\{1-0.7\exp[-j3(\varpi_1+\varpi_2)]\}$ and $1/\{1-0.7\exp[-j3(\varpi_1+\varpi_2+\varpi_3)]\}$ which represent new peak planes along $\omega_1 + \omega_2 = \pm 0.33$ and $\omega_1 + \omega_2 + \omega_3 = \pm 0.33$ in Fig. 10(d) and (e) respectively. Such changes also bring new features to the third order GFRF which is plotted in Fig. 10(a) where marked areas A, B, C and D indicate the new peak planes. Notice that the change to the

lag of the linear output term also has an influence on the numerator element of H_3, see Fig. 10(f), though not as much as it does to the elements in the denominator.

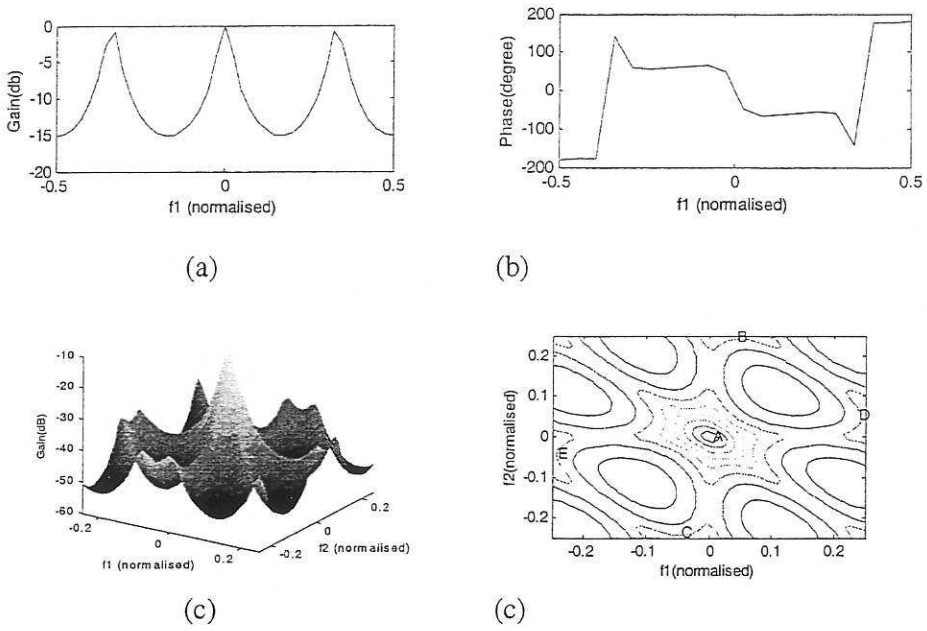

Fig. 9 The GFRFs of the system (2.11) with the $k_{10\succ 1\_1}$ changed to be 3:

(a)(b) The gain and phase of H_1;

(c) The gain of H_2; (d) The contour plot of (c).

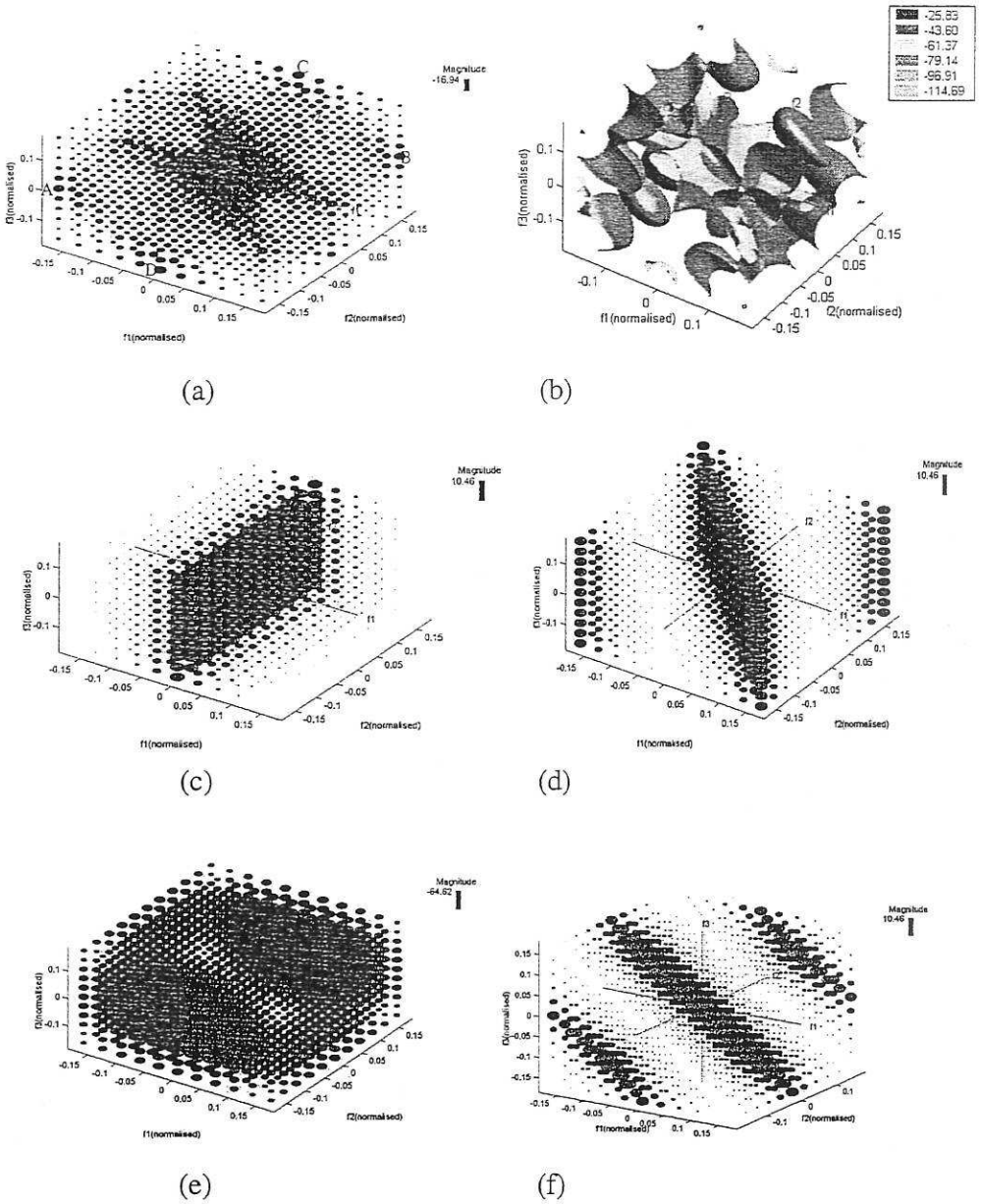

Fig. 10 The gain plots of the third order GFRF and the basic elements in (2.26)

(a)(b) the gain and the corresponding "Isosurfaces" of H_3

(c) the gain of $1/[1-0.7\exp(-j3\varpi_1)]$

(d) the gain of $1/\{1-0.7\exp[-j3(\varpi_1+\varpi_2)]\}$

(e) the gain of $1/\{1-0.7\exp[-j3(\varpi_1+\varpi_2+\varpi_3)]\}$;

(f) the gain of the numerator in (2.26)

3. Case Study Examples

3.1 A Simulation Example

Consider the Duffing oscillator, which can be expressed by

$$mD^2y + cDy + ky + k_2y^2 + k_3y^3 = x(t) \tag{2.27}$$

where $D = d/dt$ and the constant parameters are chosen as: $m = 1$, $c = 20$, $k = 10^4$, $k_2 = 10^7$ $k_3 = 5\times10^9$. In this case, the system has a resonant frequency of $f_r = \sqrt{k/m}/2\pi = 15.75Hz$. A simulation was implemented using a fourth-order Runge-Kutta algorithm under excitation by a Gaussian noise $x(t)$ of bandwidth 90Hz with r.m.s. 10.0. The input/output data were recorded at a sampling interval of 5msec. The estimation and validation methods described in Worden *et al* (1992) were employed on 1000 pairs of input/output data to yield the NARMAX model

$$\begin{aligned} y(k) &= 1.6696y(k-1) - 0.90348y(k-2) + 3.0027\times10^{-6}x(k) + 1.8040\times10^{-5}x(k-1) \\ &+2.7676\times10^{-6}x(k-2) - 218.30y^2(k-1) - 106650y^3(k-1) \end{aligned} \tag{2.28}$$

or by the new notations,

$$\begin{aligned} y(k) &= c_{10\gg1}y(k-k_{10\gg1\_1}) + c_{10\gg2}y(k-k_{10\gg2\_1}) + c_{01\gg1}x(k-k_{01\gg1\_1}) + c_{01\gg2}x(k-k_{01\gg2\_1}) \\ &+c_{01\gg3}x(k-k_{01\gg3\_1}) + c_{20\gg1}y(k-k_{20\gg1\_1})y(k-k_{20\gg1\_2}) \\ &+c_{30\gg1}y(k-k_{30\gg1\_1})y(k-k_{30\gg1\_2})y(k-k_{30\gg1\_3}) \end{aligned} \tag{2.29}$$

where

$$\begin{aligned} &c_{10\gg1} = 1.6696, c_{10\gg2} = -0.90348, c_{01\gg1} = 3.0027\times10^{-6}, c_{01\gg2} = 1.8040\times10^{-5} \\ &c_{01\gg3} = 2.7676\times10^{-6}, c_{20\gg1} = -218.30, c_{30\gg1} = -106650 \\ &k_{10\gg1\_1} = 1, k_{10\gg2\_1} = 2, k_{01\gg1\_1} = 0, k_{01\gg2\_1} = 1, k_{01\gg3\_1} = 2, k_{20\gg1\_1} = k_{20\gg1\_2} = 1 \\ &k_{30\gg1\_1} = k_{30\gg1\_2} = k_{30\gg1\_3} = 1 \end{aligned} \tag{2.30}$$

The corresponding generalised frequency response functions are obtained first from (2.4) and then the procedure of symbolic expansion is carried out to yield the expanded expression. The first three order GFRFs are given below

$$H_1(j\varpi_1) = \frac{c_{01\gg1}\exp(-j\ k_{01\gg1\_1}\varpi_1) + c_{01\gg2}\exp(-j\ k_{01\gg2\_1}\varpi_1) + c_{01\gg3}\exp(-j\ k_{01\gg3\_1}\varpi_1)}{1 - c_{10\gg1}\exp(-j\ k_{10\gg1\_1}\varpi_1) - c_{10\gg2}\exp(-j\ k_{10\gg2\_1}\varpi_1)} \tag{2.31}$$

$$\begin{aligned} &H_2^{asym}(j\varpi_1, j\varpi_2) = \\ &c_{20\gg1}[c_{01\gg1}\exp(-jk_{01\gg1\_1}\varpi_2) + c_{01\gg2}\exp(-jk_{01\gg2\_1}\varpi_2) + c_{01\gg3}\exp(-jk_{01\gg3\_1}\varpi_2)] \\ &\{c_{01\gg1}\exp[-j(k_{20\gg1\_1}\varpi_2 + (k_{20\gg1\_2} + k_{01\gg1\_1})\varpi_1)] \\ &+c_{01\gg2}\exp[-j(k_{20\gg1\_1}\varpi_2 + (k_{20\gg1\_2} + k_{01\gg2\_1})\varpi_1)] \\ &+c_{01\gg3}\exp[-j(k_{20\gg1\_1}\varpi_2 + (k_{20\gg1\_2} + k_{01\gg3\_1})\varpi_1)]\} \\ &\hline \\ &[1 - c_{10\gg1}\exp(-j\ k_{10\gg1\_1}\varpi_1) - c_{10\gg2}\exp(-j\ k_{10\gg2\_1}\varpi_1)] \\ &[1 - c_{10\gg1}\exp(-j\ k_{10\gg1\_1}\varpi_2) - c_{10\gg2}\exp(-j\ k_{10\gg2\_1}\varpi_2)] \\ &\{1 - c_{10\gg1}\exp[-j\ k_{10\gg1\_1}(\varpi_1 + \varpi_2)] - c_{10\gg2}\exp[-j\ k_{10\gg2\_1}(\varpi_1 + \varpi_2)]\} \end{aligned} \tag{2.32}$$

$$
\begin{aligned}
&H_3^{asym}(j\varpi_1, j\varpi_2, j\varpi_3) = \\
&\Big[-[c_{10>1}\exp(-jk_{01>1\_1}\varpi_1) + c_{10>2}\exp(-jk_{01>2\_1}\varpi_1) + c_{10>3}\exp(-jk_{01>3\_1}\varpi_1)] \\
&\quad [c_{10>1}\exp(-jk_{01>1\_1}\varpi_2) + c_{10>2}\exp(-jk_{01>2\_1}\varpi_2) + c_{10>3}\exp(-jk_{01>3\_1}\varpi_2)] \\
&\quad [c_{10>1}\exp(-jk_{01>1\_1}\varpi_3) + c_{10>2}\exp(-jk_{01>2\_1}\varpi_3) + c_{10>3}\exp(-jk_{01>3\_1}\varpi_3)] \\
&\quad \{-c_{20>1}^2\exp[-j\ (k_{20>1\_2}\varpi_1 + (k_{20>1\_1} + k_{20>1\_2})\varpi_2 + 2k_{20>1\_1}\varpi_3)] + \\
&\quad c_{20>1}^2 c_{10>1}\exp[-j\ ((k_{10>1\_1} + k_{20>1\_2})\varpi_1 + (k_{10>1\_1} + k_{20>1\_1} + k_{20>1\_2})\varpi_2 + 2k_{20>1\_1}\varpi_3)] + \\
&\quad c_{20>1}^2 c_{10>2}\exp[-j\ ((k_{10>2\_1} + k_{20>1\_2})\varpi_1 + (k_{10>2\_1} + k_{20>1\_1} + k_{20>1\_2})\varpi_2 + 2k_{20>1\_1}\varpi_3)] + \\
&\quad -c_{20>1}^2\exp[-j\ (2k_{20>1\_2}\varpi_1 + (k_{20>1\_1} + k_{20>1\_2})\varpi_2 + k_{20>1\_1}\varpi_3)] + \\
&\quad c_{20>1}^2 c_{10>1}\exp[-j\ (2k_{20>1\_2}\varpi_1 + (k_{10>1\_1} + k_{20>1\_1} + k_{20>1\_2})\varpi_2 + (k_{10>1\_1} + k_{20>1\_1})\varpi_3)] + \\
&\quad c_{20>1}^2 c_{10>2}\exp[-j\ (2k_{20>1\_2}\varpi_1 + (k_{10>2\_1} + k_{20>1\_1} + k_{20>1\_2})\varpi_2 + (k_{10>2\_1} + k_{20>1\_1})\varpi_3)] + \\
&\quad c_{30>1}\exp[-j(k_{30>1\_3}\varpi_1 + k_{30>1\_2}\varpi_2 + k_{30>1\_1}\varpi_3)] + \\
&\quad c_{30>1}c_{10>1}\exp[-j((k_{10>1\_1} + k_{30>1\_3})\varpi_1 + (k_{10>1\_1} + k_{30>1\_2})\varpi_2 + k_{30>1\_1}\varpi_3)] + \\
&\quad c_{30>1}c_{10>2}\exp[-j((k_{10>2\_1} + k_{30>1\_3})\varpi_1 + (k_{10>2\_1} + k_{30>1\_2})\varpi_2 + k_{30>1\_1}\varpi_3)] + \\
&\quad c_{30>1}c_{10>1}\exp[-j(k_{30>1\_3}\varpi_1 + (k_{10>1\_1} + k_{30>1\_2})\varpi_2 + (k_{10>1\_1} + k_{30>1\_1})\varpi_3)] + \\
&\quad c_{30>1}c_{10>2}\exp[-j(k_{30>1\_3}\varpi_1 + (k_{10>2\_1} + k_{30>1\_2})\varpi_2 + (k_{10>2\_1} + k_{30>1\_1})\varpi_3)] + \\
&\quad c_{30>1}c_{10>1}^2\exp[-j((k_{10>1\_1} + k_{30>1\_3})\varpi_1 + (2k_{10>1\_1} + k_{30>1\_2})\varpi_2 + (k_{10>1\_1} + k_{30>1\_1})\varpi_3)] + \\
&\quad c_{30>1}c_{10>1}c_{10>2}\exp[-j((k_{10>2\_1} + k_{30>1\_3})\varpi_1 + \\
&\quad (k_{10>1\_1} + k_{10>2\_1} + k_{30>1\_2})\varpi_2 + (k_{10>1\_1} + k_{30>1\_1})\varpi_3)] + \\
&\quad c_{30>1}c_{10>1}c_{10>2}\exp[-j((k_{10>1\_1} + k_{30>1\_3})\varpi_1 + \\
&\quad (k_{10>1\_1} + k_{10>2\_1} + k_{30>1\_2})\varpi_2 + (k_{10>2\_1} + k_{30>1\_1})\varpi_3)]\ \} \\
&\Big/ \\
&\quad [1 - c_{10>1}\exp(-j\ k_{10>1\_1}\varpi_1) - c_{10>2}\exp(-j\ k_{10>2\_1}\varpi_1)] \\
&\quad [1 - c_{10>1}\exp(-j\ k_{10>1\_1}\varpi_2) - c_{10>2}\exp(-j\ k_{10>2\_1}\varpi_2)] \\
&\quad [1 - c_{10>1}\exp(-j\ k_{10>1\_1}\varpi_3) - c_{10>2}\exp(-j\ k_{10>2\_1}\varpi_3)] \\
&\quad [1 - c_{10>1}\exp(-j\ k_{10>1\_1}(\varpi_1 + \varpi_2)) - c_{10>2}\exp(-jk_{10>2\_1}(\varpi_1 + \varpi_2))] \\
&\quad [1 - c_{10>1}\exp(-j\ k_{10>1\_1}(\varpi_2 + \varpi_3)) - c_{10>2}\exp(-jk_{10>2\_1}(\varpi_2 + \varpi_3))] \\
&\quad [1 - c_{10>1}\exp(-j\ k_{10>1\_1}(\varpi_1 + \varpi_2 + \varpi_3)) - c_{10>2}\exp(-jk_{10>2\_1}(\varpi_1 + \varpi_2 + \varpi_3))]\ \Big]
\end{aligned}
\tag{2.33}
$$

An insight into the nonlinear behaviour of the Duffing Oscillator can now be gained by investigating the GFRFs above with the aid of the graphical techniques. From eqn. (2.31), the linear FRF of the estimated Duffing oscillator has two poles corresponding to the normalised resonant frequency $f_r = \pm(15.57/200) = \pm 0.079$, which can easily be identified in the magnitude plot of H_1. This is shown in Fig. 11(a) where two resonant peaks are apparent. The linear part of the system response therefore has a maximum gain when the excitation coincides with the resonant frequency. The denominator elements of the second order GFRF in eqn. (2.32) have the same structure as H_1 and the magnitude hence possesses maxima at $f_1 = \pm 0.079$, $f_2 = \pm 0.079$ and $f_1 + f_2 = \pm 0.079$ respectively which are indicated by the

ridges in the two-dimensional magnitude plots, Fig. 12(c) (d) and (e). The maxima of the denominator elements serve as the local maxima of H_2.

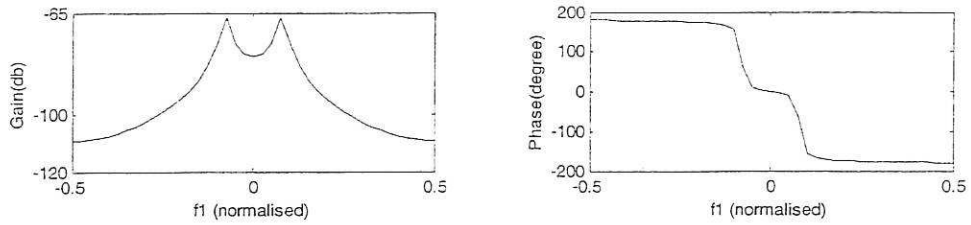

(a) (b)

Fig. 11 $H_1(j\varpi_1)$ for the estimated Duffing oscillator system (2.28): (a) Magnitude; (b) Phase

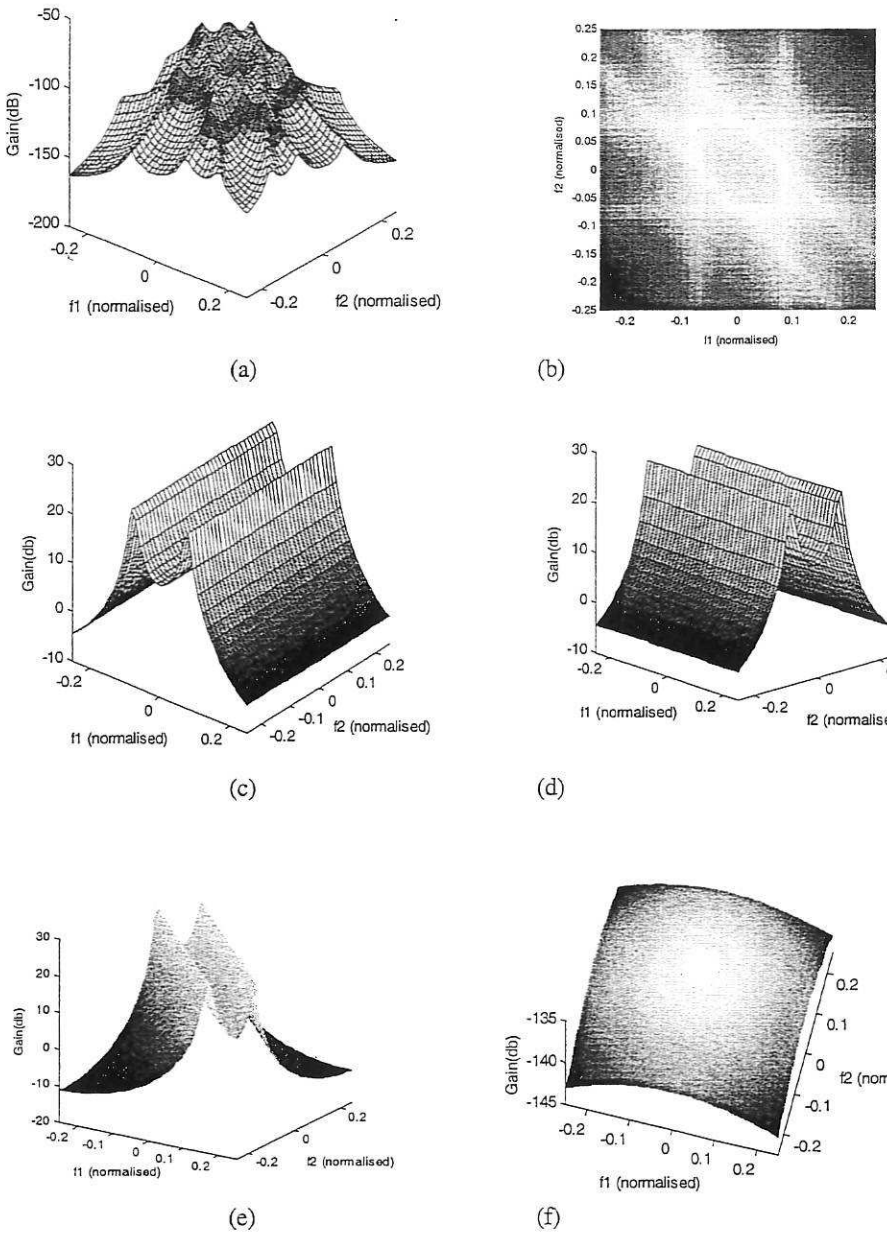

(a) (b)

(c) (d)

(e) (f)

Fig. 12 Magnitude plots of $H_2(j\varpi_1, j\varpi_2)$ for (2.32)and the constituent elements: (a)(b) Magnitude of $H_2(j\varpi_1, j\varpi_2)$ (c)(d)(e) the corresponding elements from the denominator. (f) the numerator element

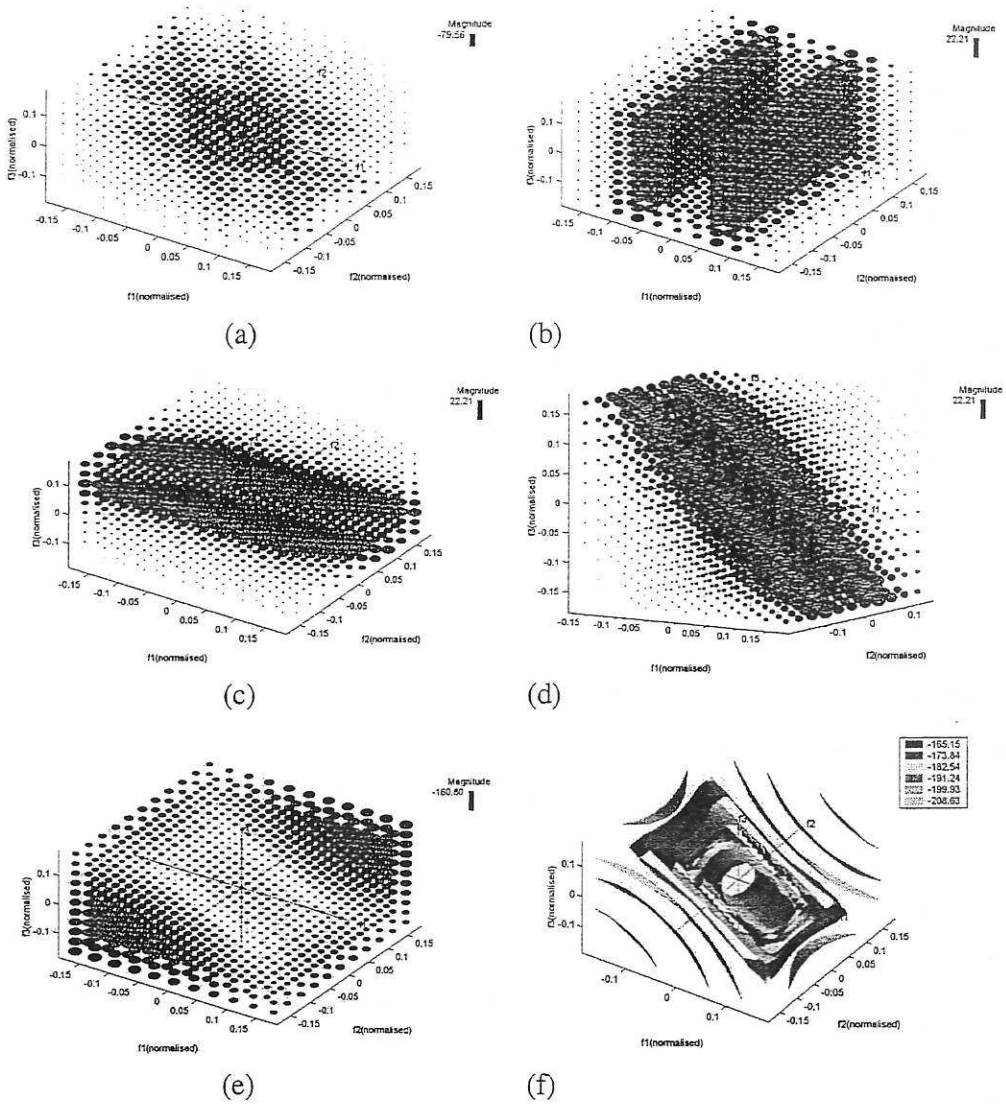

Fig. 13 Magnitude plots of $H_3(j\varpi_1, j\varpi_2, j\varpi_3)$ for (2.33) and the constituent elements: (a) Magnitude of $H_3(j\varpi_1, j\varpi_2, j\varpi_3)$; (b)(c)(d) the corresponding elements from the denominator; (e) the numerator element; (f) the Isosurface plot of the magnitude of the numerator elements

This fact is reflected in the H_2 magnitude plot where there are six ridges along the lines $f_1 = \pm 0.079$, $f_2 = \pm 0.079$ and $f_1 + f_2 = \pm 0.079$. The characteristics of H_2 indicates that there will be a significant contribution from the second order GFRF to the system output if the input contains a Duffing oscillator resonant frequency component and if any two input components conform to the relation, $f_1 + f_2 = \pm 0.079$. In this case, the energy will be transferred by intermodualtion to the output component at the resonant frequency. Fig. 12(e) shows the magnitude of the numerator element of H_2 which is an almost flat surface. This means the numerator has very little influence on the features in the magnitude of H_2, though

it does reduce the gain level of H_2. The analysis of the third order GFRF is very similar. The maxima of the denominator elements of H_3 again determine the local maxima of H_3 which are located at $f_1 = \pm 0.079$, $f_2 = \pm 0.079$, $f_3 = \pm 0.079$, $f_1 + f_2 = \pm 0.079$, $f_2 + f_3 = \pm 0.079$, $f_1 + f_2 + f_3 = \pm 0.079$. The magnitude graph of H_3 exhibits several peak planes as seen in Fig. 13(a), and these correspond to the maxima of H_3. The magnitude plots of the denominator elements help to reveal an accurate identification of the features of H_3. Fig. 13(b) indicates that for an excitation at the Duffing oscillator resonant frequency, which means $f_1 (f_2 \text{or} f_3) = \pm 0.079$, there will be a significant contribution to the system response from the third-order output y_3. It can be further observed from Fig. 13(c)(d) that input components whose frequencies meet the condition, $f_1 + f_2 = \pm 0.079$ or $f_1 + f_2 + f_3 = \pm 0.079$, will transfer energy to output components at the system resonant frequency. Fig 24(b) shows the phase of H_3

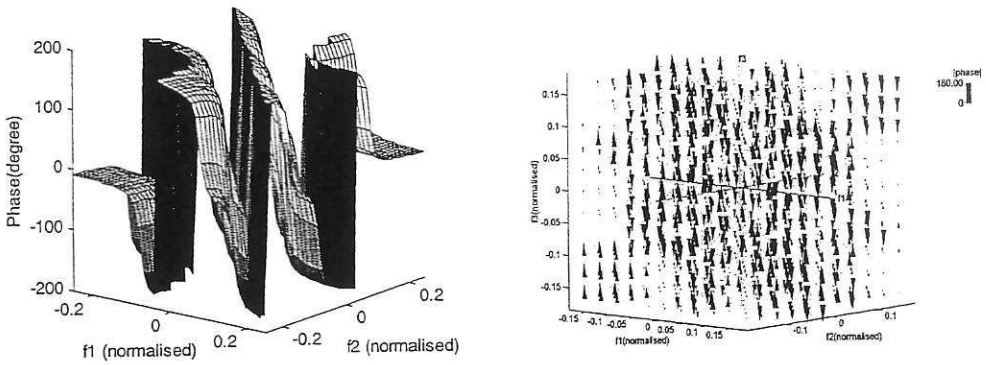

Fig. 14 Phase Response for H_2, (2.32)and H_3, (2.33): (a) H_2 phase; (b) H_3 phase

3.2 An Experimental Example Using real Data

This example relates to a study of the dynamic effects of wave forces on a large offshore structure of the type used for oil extraction in the North Sea. Worden *et al.* (1994) applied the NARMAX modelling technique to identify the wave force dynamics of U-tube, De-Voorst and Christchurch Bay data with the aim of improving the accuracy for predicting the forces. One of the results from Worden *et al.* (1994) will be used here and the new methods described above are employed to analyse the frequency response characteristics of the estimated nonlinear wave force model. A NARMAX model was fitted to the velocity (input) and force (output) data set which were measured at a sampling rate of $10Hz$ on a smooth cylinder fixed in the Delta flume of the De Voorst facility. The resulting model of the form was

$$\begin{aligned} y(k) &= c_{10\gg1} y(k - k_{10\gg1\_1}) + c_{10\gg2} y(k - k_{10\gg2\_1}) + c_{01\gg1} u(k - k_{01\gg1\_1}) + c_{01\gg2} u(k - k_{01\gg2\_1}) \\ &+ c_{01\gg3} u(k - k_{01\gg3\_1}) + c_{03\gg1} u(k - k_{03\gg1\_1}) u(k - k_{03\gg1\_2}) u(k - k_{03\gg1\_3}) \\ &+ c_{21\gg1} y(k - k_{21\gg1\_1}) y(k - k_{21\gg1\_2}) u(k - k_{21\gg1\_3}) \end{aligned} \tag{2.34}$$

where

$$
\begin{aligned}
&c_{10\gg1}=0.85124, c_{10\gg2}=-0.29028, c_{01\gg1}=-25.433, c_{01\gg2}=736.79\\
&c_{01\gg3}=-715.81, c_{03\gg1}=47.754, c_{21\gg1}=0.0010364\\
&k_{10\gg1\_1}=1, k_{10\gg2\_1}=3, k_{01\gg1\_1}=4, k_{01\gg2\_1}=0, k_{01\gg3\_1}=1, k_{03\gg1\_1}=k_{03\gg1\_2}=k_{03\gg1\_3}=4\\
&k_{21\gg1\_1}=k_{21\gg1\_2}=1, k_{21\gg1\_3}=4
\end{aligned}
\tag{2.35}
$$

The first three generalised frequency response functions of the model (2.34) are given in the expanded form as follows

$$
H_1(j\omega_1)=\frac{c_{01\gg1}\exp(-j\ \ k_{01\gg1\_1}\omega_1)+c_{01\gg2}\exp(-j\ \ k_{01\gg2\_1}\omega_1)+c_{01\gg3}\exp(-j\ \ k_{01\gg3\_1}\omega_1)}{1-c_{10\gg1}\exp(-j\ \ k_{10\gg1\_1}\omega_1)-c_{10\gg2}\exp(-j\ \ k_{10\gg2\_1}\omega_1)} \tag{2.36}
$$

$$
H_2=0
$$

$$
\begin{aligned}
H_3^{asym}(j\omega_1,j\omega_2,j\omega_3)=\exp(-jk_{03\gg1\_3}\omega_3)\times\\
\Big\{&\{c_{21\gg1}c_{01\gg1}^2\exp[-j\ \ ((k_{01\gg1\_1}+k_{21\gg1\_2})\omega_1+(k_{01\gg1\_1}+k_{21\gg1\_1})\omega_2)]+\\
&c_{21\gg1}c_{01\gg2}^2\exp[-j\ \ ((k_{01\gg2\_1}+k_{21\gg1\_2})\omega_1+(k_{01\gg2\_1}+k_{21\gg1\_1})\omega_2)]+\\
&c_{21\gg1}c_{01\gg3}^2\exp[-j\ \ ((k_{01\gg3\_1}+k_{21\gg1\_2})\omega_1+(k_{01\gg3\_1}+k_{21\gg1\_1})\omega_2]+\\
&c_{21\gg1}c_{01\gg1}c_{01\gg2}\exp[-j\ \ ((k_{01\gg1\_1}+k_{21\gg1\_2})\omega_1+(k_{01\gg2\_1}+k_{21\gg1\_1})\omega_2)]+\\
&c_{21\gg1}c_{01\gg1}c_{01\gg2}\exp[-j\ \ ((k_{01\gg2\_1}+k_{21\gg1\_2})\omega_1+(k_{01\gg1\_1}+k_{21\gg1\_1})\omega_2)]+\\
&c_{21\gg1}c_{01\gg1}c_{01\gg3}\exp[-j\ \ ((k_{01\gg1\_1}+k_{21\gg1\_2})\omega_1+(k_{01\gg3\_1}+k_{21\gg1\_1})\omega_2)]+\\
&c_{21\gg1}c_{01\gg1}c_{01\gg3}\exp[-j\ \ ((k_{01\gg3\_1}+k_{21\gg1\_2})\omega_1+(k_{01\gg1\_1}+k_{21\gg1\_1})\omega_2)]+\\
&c_{21\gg1}c_{01\gg2}c_{01\gg3}\exp[-j\ \ ((k_{01\gg2\_1}+k_{21\gg1\_2})\omega_1+(k_{01\gg3\_1}+k_{21\gg1\_1})\omega_2)]+\\
&c_{21\gg1}c_{01\gg2}c_{01\gg3}\exp[-j\ \ ((k_{01\gg3\_1}+k_{21\gg1\_2})\omega_1+(k_{01\gg2\_1}+k_{21\gg1\_1})\omega_2)]+\\
&c_{03\gg1}\exp[-j(k_{03\gg1\_1}\omega_1+k_{03\gg1\_2}\omega_2)]+\\
&c_{03\gg1}c_{10\gg1}\exp[-jk_{03\gg1\_1}\omega_1+(k_{10\gg1\_1}+k_{03\gg1\_2})\omega_2)]-\\
&c_{03\gg1}c_{10\gg1}\exp[-j((k_{03\gg1\_1}+k_{10\gg1\_1})\omega_1+k_{03\gg1\_2}\omega_2)]-\\
&c_{03\gg1}c_{10\gg2}\exp[-j((k_{10\gg2\_1}+k_{03\gg1\_1})\omega_1+k_{03\gg1\_2}\omega_2)]-\\
&c_{03\gg1}c_{10\gg2}\exp[-j(k_{30\gg1\_1}\omega_1+(k_{10\gg2\_1}+k_{03\gg1\_2})\omega_2)]-\\
&c_{03\gg1}c_{10\gg1}^2\exp[-j((k_{10\gg1\_1}+k_{03\gg1\_1})\omega_1+(k_{10\gg1\_1}+k_{03\gg1\_2})\omega_2)]+\\
&c_{03\gg1}c_{10\gg2}^2\exp[-j((k_{10\gg2\_1}+k_{03\gg1\_1})\omega_1+(k_{10\gg2\_1}+k_{03\gg1\_2})\omega_2)]+\\
&c_{03\gg1}c_{10\gg1}c_{10\gg2}\exp[-j((k_{10\gg2\_1}+k_{03\gg1\_1})\omega_1+(k_{10\gg1\_1}+k_{03\gg1\_2})\omega_2)]+\\
&c_{03\gg1}c_{10\gg1}c_{10\gg2}\exp[-j((k_{10\gg1\_1}+k_{03\gg1\_1})\omega_1+(k_{10\gg2\_1}+k_{03\gg1\_2})\omega_2)]\}\\
&\overline{[1-c_{10\gg1}\exp(-j\ \ k_{10\gg1\_1}\omega_1)-c_{10\gg2}\exp(-j\ \ k_{10\gg2\_1}\omega_1)]}\\
&[1-c_{10\gg1}\exp(-j\ \ k_{10\gg1\_1}\omega_2)-c_{10\gg2}\exp(-j\ \ k_{10\gg2\_1}\omega_2)]\\
&[1-c_{10\gg1}\exp(-j\ \ k_{10\gg1\_1}(\omega_1+\omega_2+\omega_3))-c_{10\gg2}\exp(-jk_{10\gg2\_1}(\omega_1+\omega_2+\omega_3))]\Big\}
\end{aligned}
\tag{2.37}
$$

Notice that the second order GFRF is absent in this case because there are no quadratic nonlinear terms in the time domain model. The linear FRF of the estimated nonlinear wave force dynamics is shown in Fig. 15(a) where the shape of a high-pass filter can be observed. This new feature can be attributed to the numerator element of H_1 which presents the

features of a standard high-pass filter as seen in Fig. 15(c). Another fact which can be seen from Fig. 15 (c) and (d) is that the numerator has a much higher gain level than the denominator and this confirms the leading role of the numerator element in shaping the characteristics of H_1. However, the presence of resonant peaks at $f_1 = \pm 0.0965$ in Fig. 15(a) indicates that the denominator does make its own contribution although it is not as significant as the numerator. The dominating role of the numerator element can also be found in the third order GFRF. Fig. 16(e) shows the magnitude of the numerator element of H_3, which exhibits the same number of peak areas in exactly the same positions as the magnitude of H_3 in Fig. 16(a). Both plots indicate that there will be significant effects for high frequency excitations. However, H_3 becomes more significant along $f_1 + f_2 + f_3 = \pm 0.0965$ in the high frequency range due to the contribution from the denominator elements which are shown in Fig. 16(c) and (d). This example suggests that the GFRFs of nonlinear system where the time domain model has dominant nonlinear input terms are more likely to be denominated by numerator elements rather than the denominator elements.

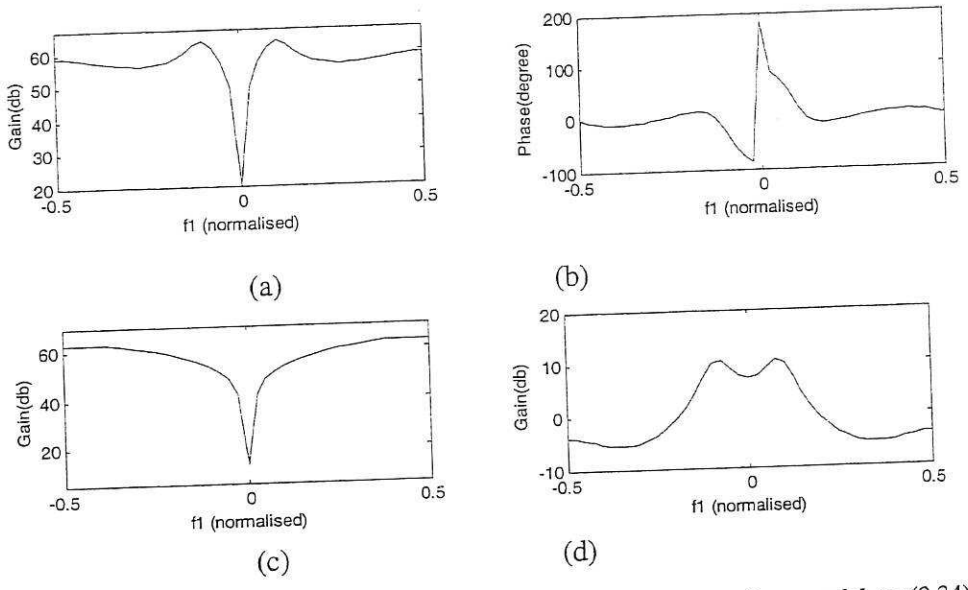

Fig. 15 $H_1(j\varpi_1)$ for the estimated dynamics of nonlinear wave force model eqn(2.34):

(a) magnitude; (b) phase; (c) magnitude of numerator; (d) magnitude of denominator

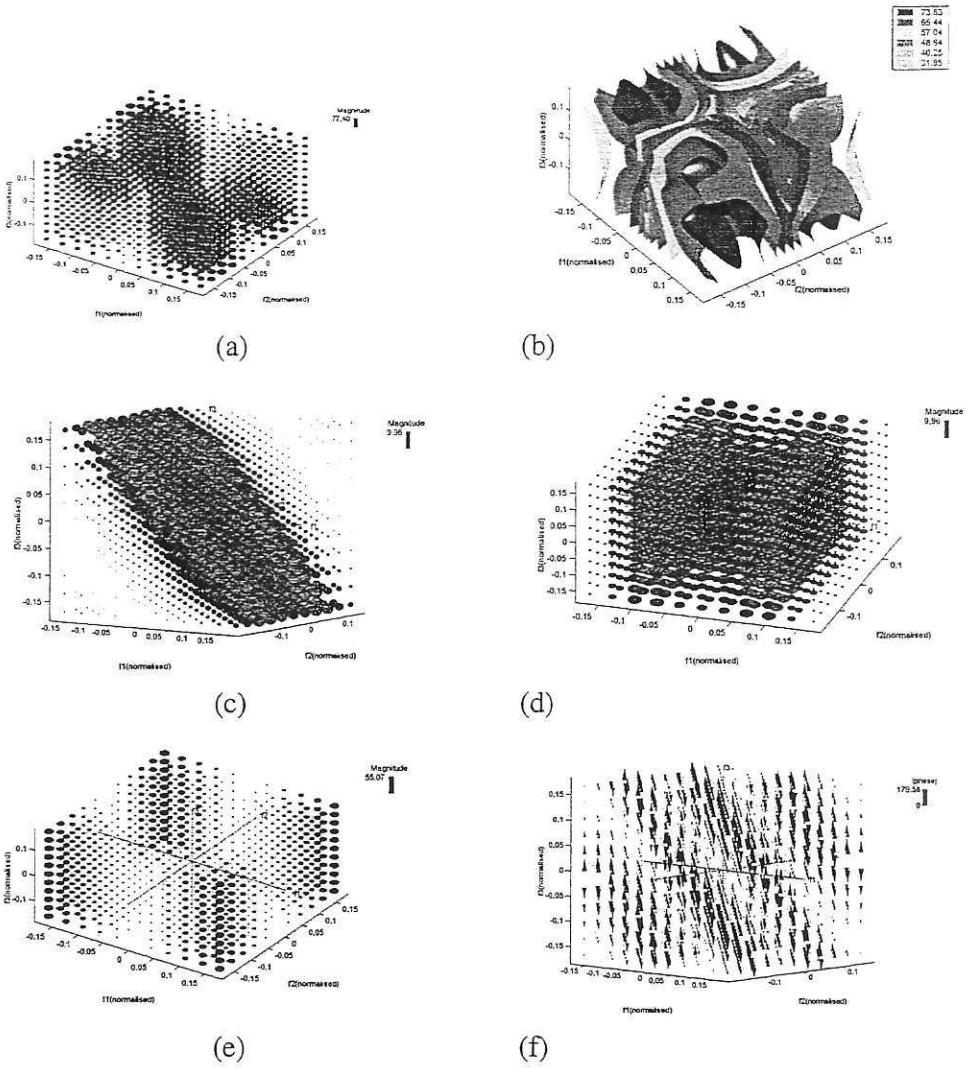

Fig. 16 H_3 for the estimated dynamics of nonlinear wave force model eqn(2.34):

(a) Magnitude of H_3 for eqn(2.37) (b) Magnitude Isosurfaces

(c) (d) Magnitude of the denominator elements of H_3

(e) Magnitude of the numerator element of H_3;

(f) Phase of H_3

4. Conclusions

A symbolic expansion technique has been introduced to give non-recursive forms to the GFRFs in terms of the nonlinear system time domain model. The structure of GFRFs can therefore be revealed in terms of new analytical expressions and the consistency on the structure can be observed. Both the results in here and from Part 1 provide new means of investigating the characteristics of generalised frequency response functions and the analysis of nonlinear systems in the frequency domain. Results using both simulated examples and real data sets show that the proposed method makes the identification of features in the GFRFs easy and straightforward. Most importantly, the effects of the time domain model terms on nonlinear system behaviours are exposed using the new approach. The analysis using the new methods on nonlinear continuous time models is related to the results above and will appear in a later publication.

Acknowledgements

S.A.B gratefully acknowledges that part of this work was supported by the UK Engineering and Physical Sciences Research Council and R.Y acknowledges the support provided by the University of Sheffield under the scholarship scheme.

References

Bedrosian, E., and Rice, S. O., 1971, The output properties of Volterra systems driven by harmonic and Gaussian inputs. *Proceedings of the Institute of Electrical and Electronics Engineers*, 59, 1688- 1707.

Bendat, J.S., 1990, Nonlinear system analysis and identification from random data. (Wiley, New York, 1990)

Billings, S. A., and Yusof, M. I., 1996, Decomposition of generalised frequency response functions for nonlinear systems using symbolic computation. *International Journal of Control*, 65, 589- 618.

Billings S.A., Zhang H., 1994, Analysing non-linear systems in the frequency domain part II: The phase response. *Mechanical Systems and Signal Processing*, 8(1), 45- 62.

Billings, S. A., and Peyton Jones, J. C., 1990, Mapping nonlinear integro-differential equation into the frequency domain. *International Journal of Control*, 52, 863- 879.

Billings S.A., Tsang K.M., 1989a, Spectral analysis for nonlinear systems Part I: Parametric nonlinear spectral analysis. *Mechanical Systems and Signal Processing*, 3, 319- 339; 1989 b, Spectral analysis for nonlinear systems Part II: Interpretation of nonlinear frequency response functions. *Mechanical Systems and Signal Processing*, 3, 341- 359.

Billings S.A, Korenberg M.J, Chen S., 1988, Identification of non-linear output-affine systems using an orthogonal least-squares algorithm. *Int.J.System Science*, 19 (8), 1559-1568, Aug

Boaghe O.M, Billings S.A., 2000, Dynamic wavelet and equivalent models. *European Journal of Control*, 6 (2), 120-131

Boyd S., Tang Y.S., and Chua L.O., 1983, Measuring Volterra Kernels. *IEEE Transactions on circuits and Systems,* Vol CAS-30, No.8, August, 571-577.

Brilliant M.B., 1958, Theory of the Analysis of Nonlinear Systems. Technical Report 345, MIT, Research Laboratory of Electronics, Cambridge, Mass, March 3.

Brillinger D.R., 1970, The identification of polynomial systems by means of high order spectra. Journal of Sound and Vibration, Vol 12, No 3, 301-331

Bussgang, J. J., Ehrman, L., and Garham, J. W., 1974, Analysis of nonlinear systems with multiple inputs. *Proceedings of the Institute of Electrical and Electronic Engineers*, 62, 1088 -1119.

Chua L.O and Ng C.Y., 1979, Frequency domain analysis of nonlinear systems: general theory. IEE Journal of Electronic Circuits and Systems. Vol 3, No.4, 165-185

Chua L.O and Liao, Y., 1989, Measuring Volterra Kernels (II). Int.J.Circuit Theory Appl., 17, 165-185, 1989

Collis W.B., White P.R. and Hammond J.K., 1998, Higher-order spectra: the bispectrum and trispectrum. *Mechanical Systems and Signal Processing,* 7(2), 173-189.

Fung C.F., Billings S.A., Luo W., 1996, On-line supervised adaptive training using radial basis function networks. NEURAL NETWORKS 9 (9) 1597-1617 Dec

George D.A., 1959, Continuous nonlinear systems. Technical Report 355, MIT Research Laboratory Of Electronics, Cambridge, Mass. July 24.

Lang Zi-Qiang, Billings S.A , 1996, Output frequency characteristics of non-linear systems. Int.J.Control, 64 (6), 1049-1067

Leontaritis I.J, Billings S.A., 1985, Input-output parametric models for nonlinear systems; Part I - Deterministic Nonlinear Systems; Part II - Stochastic Nonlinear Systems; Int.J.Control, 41, 303-359.

Kim, K. I., and Powers, E. J., 1988, A digital method of modelling quadratically nonlinear systems with a general random input. *IEEE Transactions on Acoustic, Speech and Signal Processing*, 36, 1758-1769.

Korenberg M.J, Billings S.A, Liu Y.P, Mcilroy P.J., 1988, Orthogonal parameter-estimation algorithm for non-linear stochastic-systems. Int.J.Control, 48 (1), 193-210 Jul

Nam S.W, Powers E.J., 1994, Application of higher-order spectral-analysis to cubically nonlinear-system identification. *IEEE Transactions on signal processing*, 42 (7): 1746-1765 JUL 1994

Narayanan S., 1970, Application of Volterra series to intermodulation distortion analysis of transistor feedback amplifiers. *IEEE Transactions on circuits and systems*, Vol 17, No.4, 518-527 Nov

Narayanan S., 1967, Transistor distortion analysis using Volterra series representation. Bell System Tec.J., Vol 46, No.5, 991-1024

Peyton Jones, J. C., and Billings, S. A., 1990, Interpretation of nonlinear frequency response functions. *International Journal of Control*, 52, 319-346.

Peyton Jones, J. C., and Billings, S. A., 1989, A recursive algorithm for computing the frequency response of a class of nonlinear difference equation models. *International Journal of Control*, 50, 1925-1949.

Rugh, W. J., 1981, *Nonlinear System Theory: the Volterra/Wiener Approach* (Baltimore, Maryland, U.S.A.: Johns Hopkins University Press).

Schetzen M., 1980, The Volterra and Wiener Theories of Nonlinear Systems. Chichester: John Wiley

Vinh T., Chouychai T., Liu H., and Djouder M., 1987, Second order transfer function: Computation and physical interpretation. *Proceedings of the Fifth International Model Analysis Conference*, London, U.K., pp. 587-592.

Weiner, D. D., and Spina, J. F., 1980, *Sinusoidal Analysis and Modelling of Weakly Nonlinear Circuits* (New York: Van Nostrand Reinhold).

Wiener N., 1958, Nonlinear Problems in Random Theory. MIT Press, Cambridge, Mass.

Worden K., Stansby P.K., Tomlinson G.R. and Billings S.A., 1994, Identification of non-linear wave forces. *Journal of Fluids and Structures,* 8, 19- 71.

Zhang H., Billings S.A. and Zhu Q.M., 1995, Frequency-response functions for nonlinear rational models. *International Journal of Control*, 61(5), 1073-1097.

Zhang H., Billings S.A., 1993, Analysing non-linear systems in the frequency domain part I: The transfer function. *Mechanical Systems and Signal Processing*, 7(6), 531- 550.